

Limits on the power-law mass and luminosity density profiles of elliptical galaxies from gravitational lensing systems

Shuo Cao¹, Marek Biesiada^{1,2}, Meng Yao¹, and Zong-Hong Zhu^{1*}

¹ *Department of Astronomy, Beijing Normal University, 100875, Beijing, China;*

² *Department of Astrophysics and Cosmology, Institute of Physics, University of Silesia, Uniwersytecka 4, 40-007 Katowice, Poland*

20 April 2016

ABSTRACT

We use 118 strong gravitational lenses observed by the SLACS, BELLS, LSD and SL2S surveys to constrain the total mass profile and the profile of luminosity density of stars (light-tracers) in elliptical galaxies up to redshift $z \sim 1$. Assuming power-law density profiles for the total mass density, $\rho = \rho_0(r/r_0)^{-\alpha}$, and luminosity density, $\nu = \nu_0(r/r_0)^{-\delta}$, we investigate the power law index and its first derivative with respect to the redshift. Using Monte Carlo simulations of the posterior likelihood taking the Planck’s best-fitted cosmology as a prior, we find $\gamma = 2.132 \pm 0.055$ with a mild trend $\partial\gamma/\partial z_l = -0.067 \pm 0.119$ when $\alpha = \delta = \gamma$, suggesting that the total density profile of massive galaxies could have become slightly steeper over cosmic time. Furthermore, similar analyses performed on sub-samples defined by different lens redshifts and velocity dispersions, indicate the need of treating low, intermediate and high-mass galaxies separately. Allowing δ to be a free parameter, we obtain $\alpha = 2.070 \pm 0.031$, $\partial\alpha/\partial z_l = -0.121 \pm 0.078$, and $\delta = 2.710 \pm 0.143$. The model in which mass traces light is rejected at $> 95\%$ confidence and our analysis robustly indicates the presence of dark matter in the form of a mass component that is differently spatially extended than the light. In this case, intermediate-mass elliptical galaxies ($200 \text{ km/s} < \sigma_{ap} \leq 300 \text{ km/s}$) show the best consistency with the singular isothermal sphere as an effective model of galactic lenses.

Key words: gravitational lensing: strong - galaxies: structure - cosmology: theory

1 INTRODUCTION

Since the discovery of the first strong gravitational lens system Q0957+561 (Walsh et al. 1979), strong lensing has developed into an important astrophysical tool suitable for investigating both background cosmology (Zhu 2000a,b; Chae 2003; Chae et al. 2004; Mitchell et al. 2005; Zhu & Sereno 2008a; Zhu et al. 2008b) and the structure and evolution of galaxies (Zhu & Wu 1997; Mao & Schneider 1998; Jin et al. 2000; Keeton 2001; Kochanek & White 2001; Ofek et al. 2003; Treu et al. 2006a).

A well-defined sample of strong lensing systems with accurately measured image separations and known redshifts of the lens and of the source could be useful to test cosmological parameters such as the present-day matter density Ω_m , cosmic equation of state etc. (Chae 2003; Mitchell et al. 2005) as well as the statistical properties of lensing galaxies e.g. stellar velocity dispersion function

or galaxy evolution (Chae & Mao 2003; Ofek et al. 2003). Concerning cosmological applications, the first method used for this purpose was of statistical nature. Essentially, the idea was to apply the velocity dispersion function (VDF) of early-type galaxies derived from the SDSS Data Release 5 (Sheth et al. 2010) in order to analyze the distribution of observed image separations in the sample of gravitationally lensed systems taken from Cosmic Lens All-Sky Survey (CLASS) (Mitchell et al. 2005; Zhu & Sereno 2008a; Cao & Zhu 2011a), in combination with semi-analytical modeling of galaxy formation and evolution (Chae & Mao 2003). Next, the idea of using Einstein radius measurements of strong lensing systems combined with spectroscopic data (stellar velocity dispersions) provides another interesting possibility to set limits on cosmological parameters including the cosmic equation of state (Biesiada 2006; Grillo et al. 2008; Biesiada, Piórkowska, & Malec 2010; Biesiada, Malec & Piórkowska 2011; Cao et al. 2015).

In the usual formulation of strong gravitational lensing, one often approximates the actual lens by an ide-

* zhuzh@bnu.edu.cn

alized model with a definite radial mass density profile. Most of lensing galaxies are massive early-type ellipticals as they dominate the lensing cross-sections due to their large masses. Spherically symmetric mass distribution leading to a circularly symmetric surface mass density and having analytical properties, has always been assumed in statistical studies of strong lensing systems. Such classical lens models include singular isothermal sphere (SIS) and Navarro, Frenk and White (NFW) profile (Bartelmann 1996; Navarro, Frenk, & White 1996). In particular, the SIS model with homologous profile ($\rho_{tot} \sim 1/r^2$) for the total (luminous+dark) density distribution, was extensively used in the previous lensing-based cosmological studies (Fukugita et al. 1992; Kochanek 1996; Helbig et al. 1999). This simple but well-tested mass model is strongly supported by recent observations of early-type galaxies both in the inner regions i.e. within the Einstein radii (Lagattuta et al. 2010; Ruff et al. 2011) and at larger distances of $\sim 50 - 300 h^{-1}$ kpc (Sheldon et al. 2004; Mandelbaum et al. 2006).

By assuming the isothermal mass-density profile in elliptical galaxies acting as lenses, the study of Grillo et al. (2008) reported the value for the present-day matter density lying between 0.2 and 0.3 at 99% confidence level. This early result is consistent with most of the current data: precision measurements of Type Ia supernovae (Amanullah et al. 2010), BAO cosmological distance ratios from SDSS galaxy sample (Padmanabhan et al. 2012), and the anisotropies in the cosmic microwave background radiation (Hinshaw et al. 2013; Ade et al. 2014). Currently, there is no strong and convincing evidence for deviations from the concordance Λ CDM model which invokes cosmological constant playing the role of an exotic component called dark energy responsible for more than 70% of the total energy of the universe. Latest exploration of the properties of dark energy with different astrophysical probes carried out by Cao, Liang & Zhu (2011); Cao & Zhu (2012); Cao, Covone & Zhu (2012); Cao et al. (2012); Cao, Zhu & Zhao (2012); Cao & Liang (2013); Cao & Zhu (2014) gave the results in agreement with Λ CDM. In light of phenomenological success of the concordance cosmological model, we may use gravitational lenses for a different purpose: to study the structure of galaxies (their total mass and luminosity profiles) safely assuming that the cosmological model based on current precise observations is reliable.

The deflection of light due to gravitational lensing is sensitive to the total mass of structures in the universe, independent of their nature or dynamical state. Therefore, strong gravitational lensing provides a valuable tool for measuring the mass distribution of early-type galaxies. As it is known from the gravitational lensing theory, once the critical density of the system is determined by cosmology, mass enclosed inside the Einstein radius can be directly obtained from the measurement of Einstein radius. On the other hand, by spectroscopically measuring the central stellar velocity dispersion and assuming some functional form of the mass density profile of elliptical galaxies, this mass can also be obtained through a model-dependent dynamical analysis.

Considering a more general power law model for the total mass density profile of lensing galaxies ($\rho_{tot} \sim 1/r^\gamma$), Grillo et al. (2008) presented a joint gravitational lensing and stellar-dynamical analysis of 11 early-type galax-

ies taken from the Sloan Lens ACS Survey (SLACS), and found that the total density profile of the lenses (ellipticals) is indeed well approximated by an isothermal distribution ($\gamma \sim 2$), independent of the cosmological model adopted. Using newly measured redshifts and stellar velocity dispersions from Keck spectroscopy, Ruff et al. (2011) analyzed 11 early-type galaxies (median lens redshift $z_l = 0.5$) from Strong Lenses in the Legacy Survey (SL2S). For a fixed cosmological model (Λ CDM), they derived the total mass density slope inside the Einstein radius for each lens, with an average total density slope $\gamma = 2.16 \pm 0.09$ for their sample. Using a combined set of SL2S, SLACS, and the Lenses Structure and Dynamics (LSD) survey data, a mild trend of the cosmic evolution of α was also detected, with magnitude $\partial\gamma/\partial z_l = -0.25^{+0.10}_{-0.12}$. Similar analyses aimed at establishing the evolution of mass-density profile have also been attempted in the past with negative results. For example, Koopmans et al. (2006) using the joint SLACS/LSD sample of massive lens galaxies (with velocity dispersions $\sigma_{ap} > 200$ km/s), concluded that there was no significant evolution of the total density slope inside one effective radius ($\partial\gamma/\partial z_l = 0.23 \pm 0.16$). More recently, however Bolton et al. (2012) presented an analysis of a combined sample of SLACS and BELLS lenses with the conclusion that galaxies at lower redshifts tend to have steeper mass profiles at a later cosmic times ($\partial\gamma/\partial z_l = -0.60 \pm 0.15$). This is consistent with the newest results obtained by Sonnenfeld et al. (2013b) from enlarged sample observed by SL2S combined with SLACS ($\partial\gamma/\partial z_l = -0.31 \pm 0.10$).

Given the previous literature listed above (Koopmans et al. 2006; Grillo et al. 2008; Ruff et al. 2011; Bolton et al. 2012; Sonnenfeld et al. 2013b), the primary motivation of this work is to develop a reliable phenomenological model of early-type lensing galaxies suitable for further cosmological studies. It is only quite recently when reasonable catalogs of strong lenses: containing more than 100 lenses, with spectroscopic as well as astrometric data, obtained with well defined selection criteria are becoming available. The purpose of this work is to use the new sample of 118 lenses (Cao et al. 2015) compiled from SLACS, BELLS, LSD, and SL2S to provide independent constraints on the mass distribution of early-type galaxies. We consider a general power-law mass density profile allowing the power-law index to evolve with redshift. Moreover, we also relax the rigid assumption that the stellar luminosity and total mass distributions follow the same power-law. In Section 2 we briefly describe the methodology of subsequent analysis, the sample and its construction. The results obtained with the full sample and on several sub-samples are presented in Section 3. The main conclusions are summarized in Section 4. Throughout this paper we assume flat Λ CDM cosmology based on the recent Planck observations, with $\Omega_m = 0.315$ and $h = 0.673$ (Ade et al. 2014).

2 METHOD AND DATA

From the theory of gravitational lensing it follows that, for a specific strong lensing system, multiple images can only form close to the so-called Einstein ring θ_E (Schneider et al. 1992). In the case of circularly symmetric mass distribution,

the mass M_E enclosed within a cylinder of a radius equal to the Einstein radius is also directly related to the geometry of the Universe (through angular-diameter distances):

$$\theta_E = \left(\frac{4GM_E}{c^2} \frac{D_{ls}}{D_s D_l} \right)^{1/2}. \quad (1)$$

Here, D_s is the angular-diameter distance to the source, D_l is the distance to the lens, and D_{ls} is the distance between the lens and the source. Throughout this paper we will use angular-diameter distances, unless stated otherwise.

Rearranging terms using $R_E = D_l \theta_E$ (R is the cylindrical radius perpendicular to the line of sight, \mathcal{Z} -axis), we obtain a useful formula

$$\frac{GM_E}{R_E} = \frac{c^2}{4} \frac{D_s}{D_{ls}} \theta_E, \quad (2)$$

which indicates that only mass inside the Einstein radius has net effect on the deflection of light, regardless of the full lens mass distribution.

On the other hand, the measurement of central velocity dispersion σ can provide a model-dependent dynamical estimate of this mass based on the assumption of the power-law mass density profile ρ , and luminosity density of stars ν (Koopmans 2006):

$$\rho(r) = \rho_0 \left(\frac{r}{r_0} \right)^{-\alpha} \quad (3)$$

$$\nu(r) = \nu_0 \left(\frac{r}{r_0} \right)^{-\delta} \quad (4)$$

Here r is the spherical radial coordinate from the lens center and it is related to the projected radial coordinate R and the coordinate along the line of sight \mathcal{Z} by: $r^2 = R^2 + \mathcal{Z}^2$. In order to characterize the anisotropic distribution of three-dimensional velocity dispersion, an anisotropy parameter β is also introduced:

$$\beta(r) = 1 - \sigma_t^2 / \sigma_r^2 \quad (5)$$

where σ_t and σ_r are the tangential and radial velocity dispersions, respectively. It has almost always been assumed to be independent of r (Bolton, Rappaport & Burles 2006; Koopmans 2006). In our analysis we will consider two cases: isotropic distribution $\beta = 0$ and anisotropic distribution $\beta = \text{const.} \neq 0$. We emphasize here that the power-law model adopted by us for the luminosity profile is simply a convenient and flexible parameterized mathematical model for early-type galaxies. In the previous work by Bolton et al. (2012), it was verified that the results of mass-density profile evolution do not depend significantly on the choice of the specific form of parameterized luminosity-profile. Taking the Nuker profile (Lauer et al. 1995), a broken power-law profile including a transition of variable softness between inner and outer regions, as the reference model they found that differences between constraints obtained with the Nuker and de Vaucouleurs (de Vaucouleurs 1948) profiles were insignificant. However, in order to better describe the distribution of luminous tracers in galaxies, more data-orientated luminosity profiles like de Vaucouleurs, Hernquist, Jaffe or Nuker profiles (see e.g. Koopmans et al. (2006); Bolton et al. (2012); Sonnenfeld et al. (2013b)) should be taken into consideration in our next-step works.

Following the well-known spherical Jeans equation

(Binney 1980), radial velocity dispersion of luminous matter $\sigma^2(r)$ of the early-type galaxies can be expressed as

$$\sigma_r^2(r) = \frac{G \int_r^\infty dr' \nu(r') M(r') (r')^{2\beta-2}}{r^{2\beta} \nu(r)}, \quad (6)$$

where β is the above mentioned anisotropy parameter. Using the mass density profile from Eq. (3), one can obtain the relation between M_E and the mass enclosed within a spherical radius r :

$$M(r) = \frac{2}{\sqrt{\pi} \lambda(\alpha)} \left(\frac{r}{R_E} \right)^{3-\alpha} M_E, \quad (7)$$

where $\lambda(x) = \Gamma(\frac{x-1}{2}) / \Gamma(\frac{x}{2})$ denotes the ratio of Euler's gamma functions. Using the notation $\xi = \delta + \alpha - 2$, after Koopmans (2006), we obtain a convenient form for the radial velocity dispersion by scaling the dynamical mass to the Einstein radius:

$$\sigma_r^2(r) = \left[\frac{GM_E}{R_E} \right] \frac{2}{\sqrt{\pi} (\xi - 2\beta) \lambda(\alpha)} \left(\frac{r}{R_E} \right)^{2-\alpha} \quad (8)$$

A key ingredient in all measurements concerning strong lensing systems is the *observed* velocity dispersion, which is a projected, luminosity weighted average of the radially-dependent velocity dispersion profile of the lensing galaxy. In order to predict this value based on a set of galaxy parameters, we start with Eq. (6). Note that this equation is valid when the relationship between stellar number density and stellar luminosity density is spatially constant, an assumption unlikely to be violated appreciably within the effective radius of the early-type lens galaxies under consideration.

Furthermore, the actual observed velocity dispersion is measured over the spectrometer aperture θ_{ap} blurred with atmospheric seeing. In our analysis, we will apply the aperture weighting function provided by Schwab et al. (2010)

$$w(R) \approx e^{-R^2/2\bar{\sigma}_{\text{atm}}^2}, \quad (9)$$

where

$$\bar{\sigma}_{\text{atm}} \approx \sigma_{\text{atm}} \sqrt{1 + \chi^2/4 + \chi^4/40} \quad (10)$$

$\chi = \theta_{\text{ap}}/\sigma_{\text{atm}}$ and σ_{atm} is the seeing recorded by the spectroscopic guide cameras during survey observations. Considering the effects of aperture with atmospheric blurring and luminosity-weighted averaging (see Schwab et al. (2010) for details), the observed velocity dispersion can be expressed as

$$\begin{aligned} \bar{\sigma}_*^2 &= \left[\frac{c^2}{4} \frac{D_s}{D_{ls}} \theta_E \right] \frac{2}{\sqrt{\pi}} \frac{(2\bar{\sigma}_{\text{atm}}^2/\theta_E^2)^{1-\alpha/2}}{(\xi - 2\beta)} \\ &\times \left[\frac{\lambda(\xi) - \beta\lambda(\xi + 2)}{\lambda(\alpha)\lambda(\delta)} \right] \frac{\Gamma(\frac{3-\xi}{2})}{\Gamma(\frac{3-\delta}{2})}. \end{aligned} \quad (11)$$

The observed stellar velocity dispersion is a luminosity-weighted average dispersion inside the fiber aperture. Spectroscopic data obtained in different surveys comprise luminosity averaged line-of-sight velocity dispersions σ_{ap} measured inside different apertures. According to Cao et al. (2015), whose compilation of lenses is used in this paper, SLACS and BELLS source papers reported effective circular apertures, while for the SL2S and LSD surveys they have been assessed from the sizes of the slit reported in source papers. In our analysis, we take for σ_{atm} the median value recorded by the spectroscopic guide

cameras during survey observations. More specifically, we have added $1''.4$ seeing for the SLACS spectroscopic observations according to Bolton et al. (2008) and $1''.8$ seeing for the BOSS spectroscopic observations according to Bolton et al. (2012); Shu et al. (2015). For the SL2S sample the seeing for each individual lens was taken after Sonnenfeld et al. (2013b). In the case of LSD systems: CFRS03-1077, HST14176 and HST15433 the seeing data were taken from Treu & Koopmans (2004). Since they reported two seeing values per lens, we have taken the median. For Q0047-281 we took the seeing value after Koopmans & Treu (2003), but for MG2016+112 we assumed $0''.8$ seeing because there was no seeing reported in the source paper.

From the above equation, one can immediately observe that there are degeneracies among α , β and δ . More importantly, if we accurately knew the distance ratio D_s/D_{ls} , we could get more stringent constraints on the parameters α and δ describing the mass distribution of lensing galaxies. In our analysis, the angular diameter distance $D_{12}(z)$ between redshifts z_1 and z_2 (expressed in Mpc and assuming flat FRW metric) is calculated as

$$D_{12} = \frac{c}{H_0(1+z_2)} \int_{z_1}^{z_2} \frac{dz'}{E(z'; \Omega_m)} \quad (12)$$

where $E(z; \Omega_m) = \sqrt{\Omega_m(1+z)^3 + (1-\Omega_m)}$ is the dimensionless Hubble function in flat Λ CDM model. We use the best-fitted matter density parameter Ω_m given by Planck Collaboration: $\Omega_m = 0.315$ (Ade et al. 2014). Because our expressions involve only distance ratios D_{ls}/D_s , the Hubble constant cancels and we do not have to use its value, which according to Planck ($H_0 = 67.3 \text{ km s}^{-1} \text{ Mpc}^{-1}$) was somewhat discrepant with alternative estimates.

In order to determine (α, δ) parameters of lensing galaxies, we used Markov chain Monte Carlo (MCMC) method to sample their probability density distributions based on the likelihood $\mathcal{L} \sim \exp(-\chi^2/2)$, where

$$\chi^2 = \sum_{i=1}^{118} \left(\frac{\bar{\sigma}_{*,i}(z_{l,i}, z_{s,i}, \theta_{E,i}, \theta_{ap,i}, \sigma_{atm}; \alpha, \beta, \delta) - \sigma_{ap,i}}{\Delta \bar{\sigma}_{*,i}} \right)^2 \quad (13)$$

was calculated using the measured values of velocity dispersion σ_{ap} , Einstein radius θ_E , and aperture radius θ_{ap} . Following the SLACS team we took the fractional uncertainty of the Einstein radius at the level of 5%, redshift measurements were assumed to be accurate. The uncertainties of σ_{ap} and θ_E were propagated to the final uncertainty $\Delta \bar{\sigma}_*$ of $\bar{\sigma}_*$. However, the statistical error on Einstein radius was relatively small in comparison to the velocity dispersion error.

In this paper, we used a comprehensive compilation of 118 strong lensing systems observed by four surveys: SLACS, BELLS, LSD and SL2S, which is also the largest gravitational lens sample (suitable for the purpose of this study) published in our recent work (Cao et al. 2015). The SLACS data comprise 57 strong lenses presented in Bolton et al. (2008); Auger et al. (2009), the BELLS data comprise 25 lenses taken from Brownstein et al. (2012), then 5 most reliable lenses from the LSD survey were taken after Koopmans & Treu (2003); Treu & Koopmans (2002, 2004), and the SL2S data for a total of 31 lenses were taken from Sonnenfeld et al. (2013a,b). Scatter plot showing the distribution of lenses from different surveys in the redshift-

velocity dispersion space can be seen in Fig. 1 of Cao et al. (2015), from which one can see a fair coverage of redshifts in the combined sample. We remind the readers to refer to Table 1 of Cao et al. (2015) for the full information about all the 118 lenses. Because our list includes lensing galaxies corresponding to different velocity dispersions at different redshifts, so besides the full combined sample we also considered six sub-samples separately. Within a singular isothermal sphere model, the dynamical mass is related to the velocity dispersion through the relation $M \propto \sigma^2$ (Longair 1998). Therefore, we considered three sub-samples defined by the velocity dispersions of lenses ¹: $\sigma_{ap} \leq 200 \text{ km/s}$ ($n = 25$ lenses), $200 \text{ km/s} < \sigma_{ap} \leq 300 \text{ km/s}$ ($n = 80$ lenses), and $\sigma_{ap} > 300 \text{ km/s}$ ($n = 13$ lenses). Another set of three sub-samples was defined by restriction to three redshift ranges ²: $z \leq 0.20$ ($n = 25$ lenses), $0.20 < z \leq 0.50$ ($n = 65$ lenses), and $z > 0.5$ ($n = 28$ lenses).

3 RESULTS AND DISCUSSIONS

In this paper, we focused on constraining the parameters (α, δ) characterizing the structure of elliptical galaxies using different samples of strong lensing systems, i.e. the full $n = 118$ sample as well as six sub-samples defined with different selection criteria. These parameters are assumed to be the same for all lenses, and we used MCMC method based on the publicly available CosmoMC package (Lewis & Bridle 2002) to sample their probability density distributions. To be specific, we generated eight chains and stopped sampling when the worst e-value [the variance(mean)/mean(variance) of $1/2$ chains] $R-1$ is of the order 0.01.

3.1 The case with $\alpha = \delta = \gamma$

In the first case analysed, we assume that the radial profile of the luminosity density (ν) follows that of the total mass density (ρ), i.e., $\alpha = \delta = \gamma$, and both of them evolve as a function of redshift:

$$\gamma(z) = \gamma_0 + \gamma_1 z, \quad (14)$$

where γ_0 is the present-day value and γ_1 characterizes the evolution of γ with redshift. In order to make comparison with the previous results, we assume that stellar velocity anisotropy vanishes $\beta = 0$. Using the full data-set, we obtain the following best-fit values and corresponding 1σ uncertainties

$$\begin{aligned} \gamma_0 &= 2.132 \pm 0.055, \\ \gamma_1 &= -0.067 \pm 0.119. \end{aligned}$$

¹ As a rough criterion, elliptical galaxies with velocity dispersion smaller than 200 km/s are classified as relatively low-mass galaxies, while those with velocity dispersion larger than 300 km/s are treated as relatively high-mass galaxies.

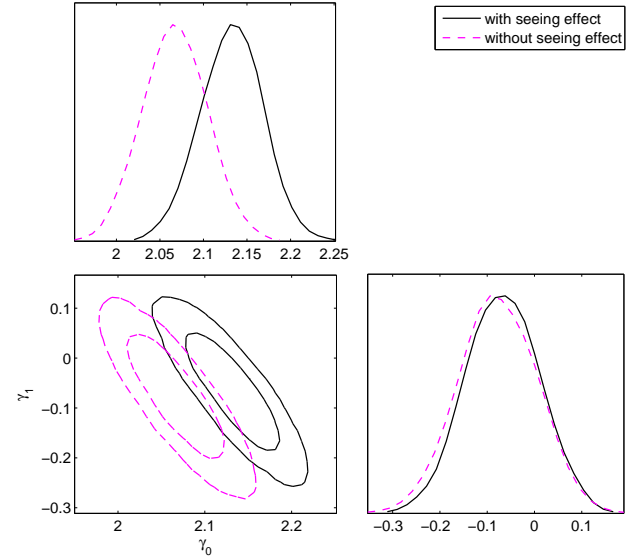
² In the full sample of 118 strong lenses, the highest lens redshift of $z_l = 1.00$ was recorded for the system MG2016. Therefore, we set the breakpoints at $1/2$ and $1/5$ of the highest redshift, that is at $z_l = 0.50$ and $z_l = 0.20$ respectively. We remark here that such an approach does not represent any physical aspects of galaxy distribution in redshift, but it guarantees that there are enough data points in each sub-sample.

Table 1. Summary of constraints on the galaxy structure parameters obtained with the full sample and six sub-samples of strong lensing systems (see text for definitions).

Sample (Model)	Galaxy structure parameters $\{\gamma, \alpha, \delta\}$
Full sample ($\alpha = \delta = \gamma$)	$\gamma_0 = 2.132 \pm 0.055$ (1σ), $\gamma_1 = -0.067 \pm 0.119$ (1σ)
Full sample ($\alpha \neq \delta$)	$\alpha_0 = 2.070 \pm 0.031$ (1σ), $\alpha_1 = -0.121 \pm 0.078$ (1σ), $\delta = 2.710 \pm 0.143$ (1σ)
Full sample ($\alpha \neq \delta$)	$\alpha = 2.035 \pm 0.013$ (1σ), $\delta = 2.681 \pm 0.164$ (1σ)
Sub-sample ($z \leq 0.2$) ($\alpha = \delta = \gamma$)	$\gamma_0 = 2.175^{+0.105}_{-0.218}$ (1σ), $\gamma_1 = -0.495^{+1.345}_{-0.565}$ (1σ)
Sub-sample ($0.2 < z \leq 0.5$) ($\alpha = \delta = \gamma$)	$\gamma_0 = 2.093 \pm 0.114$ (1σ), $\gamma_1 = 0.063 \pm 0.307$ (1σ)
Sub-sample ($z > 0.5$) ($\alpha = \delta = \gamma$)	$\gamma_0 = 2.275 \pm 0.269$ (1σ), $\gamma_1 = -0.288 \pm 0.394$ (1σ)
Sub-sample ($\sigma_{ap} \leq 200$ km/s) ($\alpha = \delta = \gamma$)	$\gamma_0 = 2.135 \pm 0.087$ (1σ), $\gamma_1 = 0.012 \pm 0.204$ (1σ)
Sub-sample (200 km/s $< \sigma_{ap} \leq 300$ km/s) ($\alpha = \delta = \gamma$)	$\gamma_0 = 2.115 \pm 0.072$ (1σ), $\gamma_1 = -0.091 \pm 0.154$ (1σ)
Sub-sample ($\sigma_{ap} > 300$ km/s) ($\alpha = \delta = \gamma$)	$\gamma_0 = 1.982 \pm 0.154$ (1σ), $\gamma_1 = -0.047 \pm 0.350$ (1σ)
Sub-sample ($z \leq 0.2$) ($\alpha \neq \delta$)	$\alpha = 2.067^{+0.077}_{-0.140}$ (1σ), $\delta = 2.410^{+0.410}_{-0.242}$ (1σ)
Sub-sample ($0.2 < z \leq 0.5$) ($\alpha \neq \delta$)	$\alpha = 2.029 \pm 0.018$ (1σ), $\delta = 2.700 \pm 0.180$ (1σ)
Sub-sample ($z > 0.5$) ($\alpha \neq \delta$)	$\alpha = 1.982 \pm 0.044$ (1σ), $\delta = 2.731 \pm 0.216$ (1σ)
Sub-sample ($\sigma_{ap} \leq 200$ km/s) ($\alpha \neq \delta$)	$\alpha = 1.754 \pm 0.179$ (1σ), $\delta = 2.660 \pm 0.120$ (1σ)
Sub-sample (200 km/s $< \sigma_{ap} \leq 300$ km/s) ($\alpha \neq \delta$)	$\alpha = 2.004 \pm 0.065$ (1σ), $\delta = 2.539 \pm 0.279$ (1σ)
Sub-sample ($\sigma_{ap} > 300$ km/s) ($\alpha \neq \delta$)	$\alpha = 1.829 \pm 0.190$ (1σ), $\delta = 2.101 \pm 0.149$ (1σ)

Marginalized 1σ and 2σ contours for each parameter are shown in Fig. 1. The results reveal compatibility between our full lens sample and a smaller combined sample from SLACS, SL2S and LSD used previously by Ruff et al. (2011); Sonnenfeld et al. (2013b). Our results suggest that the total density profile of early-type galaxies has become slightly steeper over cosmic time ($z \sim 1$), which might indicate the effect of dissipative processes in the growth of massive galaxies. It is interesting to see the difference in the final results obtained with and without seeing taken into account. Therefore, Fig. 1 also shows the the limits in the plane of γ_0 and γ_1 based on the full sample of lenses without accounting for seeing (see Koopmans (2006) for details). In such a case, we have $\gamma_0 = 2.066 \pm 0.057$ and $\gamma_0 = -0.077 \pm 0.126$, which is consistent with the singular isothermal sphere ($\gamma_0 = 2$, $\gamma_1 = 0$) model within 1σ .

In Table 1 and Fig. 2-3, we also show the results for γ_0 and γ_1 obtained on six sub-samples described in Section 2. Concerning the sub-samples with different lens redshift bins, we find that constraints coming from the three sub-samples are in perfect agreement with each other. It is good to recall (Cao et al. 2015) the median values of the lens redshifts for different surveys: SLACS – $z_l = 0.215$, BELLS – $z_l = 0.517$, LSD – $z_l = 0.81$ and SL2S – $z_l = 0.456$. Note that SL2S survey would be particularly promising in the future since it has already reached the maximum lens redshift of $z_l = 0.80$. For other three sub-samples of lenses differing by velocity dispersions (which is directly related to the masses of galaxies, $M \propto \sigma^2$), we note that the ranges of γ parameters for relatively low-mass galaxies ($\gamma_0 = 2.135 \pm 0.087$, $\gamma_1 = 0.012 \pm 0.204$) are close to estimates obtained for intermediate-mass elliptical galaxies ($\gamma_0 = 2.115 \pm 0.072$, $\gamma_1 = -0.091 \pm 0.154$). The best-fit values of γ_0 and γ_1 for massive galaxies ($\gamma_0 = 1.982 \pm 0.154$, $\gamma_1 = -0.047 \pm 0.350$) are significantly different from the corresponding quantities of low-mass and intermediate-mass elliptical galaxies. On the other hand, the singular isothermal sphere model (SIS)


Figure 1. Constraints on the total-mass density parameter obtained from the full sample of strong lensing systems (Solid line). Limits in the plane of γ_0 and γ_1 without using the seeing observations are also shown for comparison (Dashed line).

is only consistent with results obtained in massive (high velocity dispersion) galaxies. The SIS value of $\gamma = 2$ is indeed very close to the central fit values. Consequently, our results imply that the mass-density profile is different in low, intermediate and high-mass elliptical galaxies. This implies the need of treating these classes of galaxies separately.

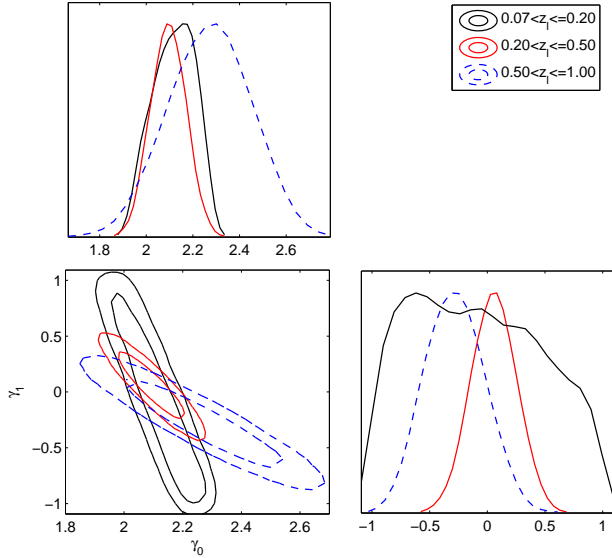


Figure 2. Constraints on the total-mass density parameter obtained from sub-sample of strong lenses defined by three different redshift bins.

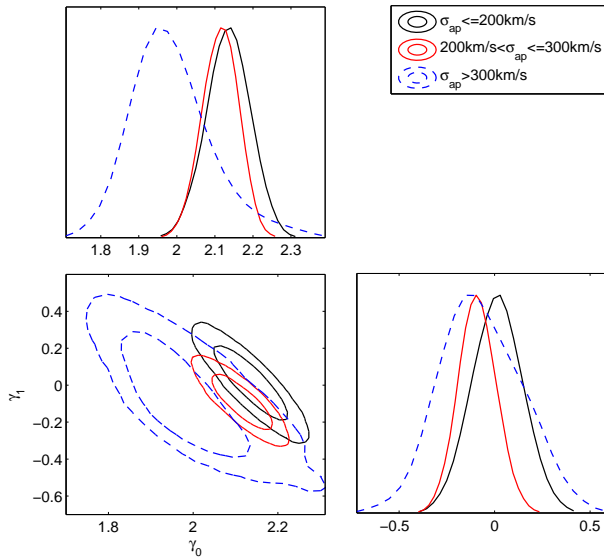


Figure 3. Constraints on the total-mass density parameter obtained from three sub-samples of strong lenses selected according to their velocity dispersions.

3.2 The case with $\alpha \neq \delta$

In the second case, we allow the luminosity density profile to be different from the total-mass density profile, i.e., $\alpha \neq \delta$, and the stellar velocity anisotropy exists, i.e., $\beta \neq 0$. Moreover, we characterize anisotropy β by a Gaussian distribution, $\beta = 0.18 \pm 0.13$, based on the well-studied sample of nearby elliptical galaxies from Gerhard et al. (2001). The above cited uncertainty $\sigma_\beta = 0.13$ represents the intrinsic spread of this quantity (Bolton, Rappaport & Burles 2006; Schwab et al. 2010). In order to alleviate the degeneracy

between luminosity density and total-mass density profiles, which might yield more meaningful results, we firstly include the redshift evolution of the mass-density slope $\alpha = \alpha_0 + \alpha_1 z$ where α is not equal to δ (the luminosity-density slope). Performing fits on the full data-set, the 68% confidence level uncertainties on the three model parameters are

$$\begin{aligned}\alpha_0 &= 2.070 \pm 0.031, \\ \alpha_1 &= -0.121 \pm 0.078, \\ \delta &= 2.710 \pm 0.143.\end{aligned}$$

Fig. 4 shows these constraints in the parameter space of α_0 , α_1 and δ . It is interesting to note that the values of mass-density exponents are inconsistent with the values obtained in the case of $\alpha = \delta$. This implies that from the point of view of stellar dynamics, the effective description of mass distribution in lensing galaxies can be much different when $\alpha \neq \delta$. Moreover, the obtained value of δ is consistent with that of Schwab et al. (2010), which fit the PSF convolved two-dimensional power-law ellipsoid images of 53 SLACS lenses to their corresponding HST F814W imaging data within a circle of radius (Bolton, Rappaport & Burles 2006). However, we also notice that all of these three parameters have relatively large uncertainties. In order to obtain more stringent results, we will further ignore the redshift evolution of the mass-density slope $\alpha_1 = 0$.

Performing fits on the full data-set, we obtain the following best-fit values and corresponding 68% confidence level uncertainties

$$\begin{aligned}\alpha &= 2.035 \pm 0.013, \\ \delta &= 2.681 \pm 0.164.\end{aligned}$$

From the results displayed in Fig. 5, one can see that the power-law exponent δ , which describes the luminosity density profile of elliptical galaxies, takes values from the range which is different from the range of mass-density exponent α . Our result is also in good agreement with a recent analysis of lensing statistics by Schwab et al. (2010), which reported mean value of $\langle \delta \rangle = 2.40$ and a standard deviation $\sigma_\delta = 0.11$. The different range of (α, δ) parameters reveals differences in mass density distributions of dark matter and luminous baryons in early-type galaxies. A model in which mass traces light ($\alpha = \delta$) is rejected at $> 95\%$ confidence and our analysis robustly indicates the presence of dark matter in the form of a mass component that is differently spatially distributed than stars.

From the results obtained on six sub-samples shown in Fig. 6-7, one can see again the consistency between three sub-samples defined according to the lens redshift bins. Concerning the sub-samples differing by velocity dispersion (i.e. by mass as well) both the total-mass and luminosity distributions exhibit different density profiles across sub-samples. The constraint results on α parameter are particularly interesting. Namely, one can see that samples of elliptical galaxies differing by mass have different power-law profiles of total-mass density distribution: $\alpha = 1.754 \pm 0.179$ for $\sigma_{ap} \leq 200$ km/s, $\alpha = 2.004 \pm 0.065$ for $200 \text{ km/s} < \sigma_{ap} \leq 300$ km/s, and $\alpha = 1.829 \pm 0.190$ for $\sigma_{ap} > 300$ km/s. Substantial distinction between α and δ parameters exists for all three sub-populations within 1σ . It is of interest to note that the intermediate-mass elliptical galaxies are consistent with the singular isothermal sphere within 1σ region. Taking the lu-

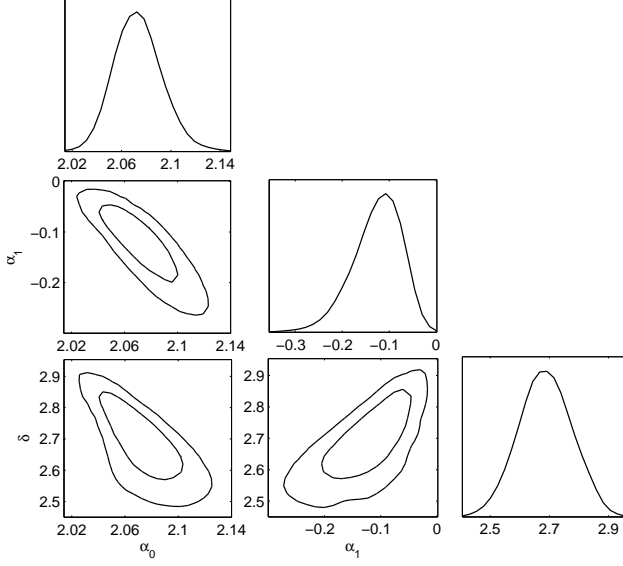


Figure 4. Constraints on the total-mass and luminosity density parameters obtained from the full sample of strong lensing systems. Redshift evolution of the mass-density slope is parameterized as $\alpha = \alpha_0 + \alpha_1 z$.

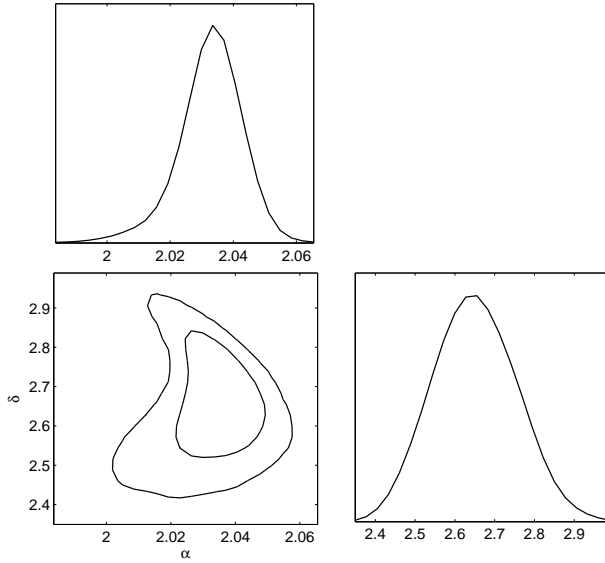


Figure 5. Constraints on the total-mass and luminosity density parameters obtained from the full sample of strong lensing systems.

minosity profile of elliptical galaxies into consideration, the obtained value of δ from our sub-sample with intermediate velocity dispersion ($200 \text{ km/s} < \sigma_{ap} \leq 300 \text{ km/s}$), whose confidence contours in (α, δ) parameter plane differ the other two remaining samples, is in perfect agreement with the previous results from smaller SLACS sample (Schwab et al. 2010).

Previously, some researchers (Auger et al. 2010; Sonnenfeld et al. 2013b; Dutton & Treu 2014) have considered the problem of how does the mass weighted slope

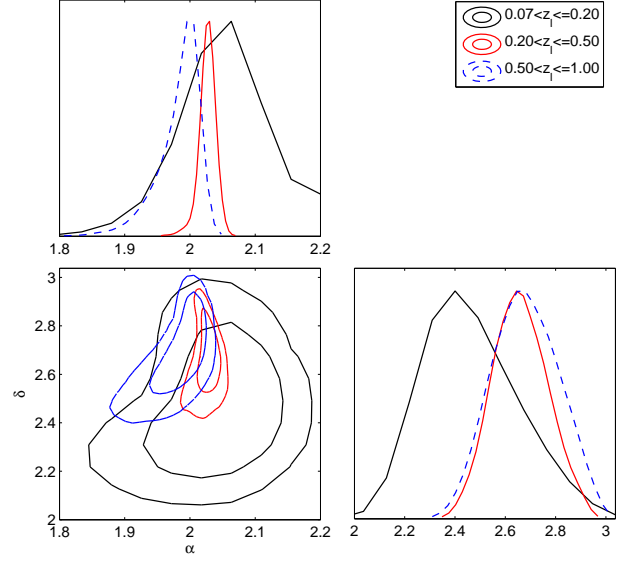


Figure 6. Constraints on the total-mass and luminosity density parameters obtained from sub-samples of strong lensing systems defined by three different redshift bins.

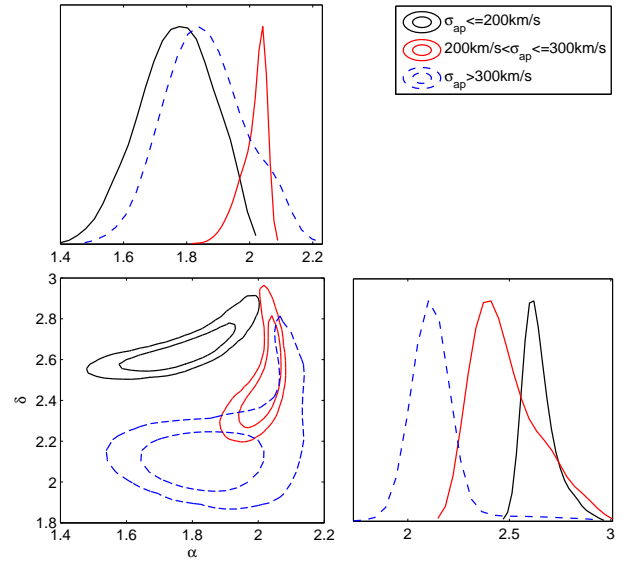


Figure 7. Constraints on the total-mass and luminosity density parameters obtained from three sub-samples of strong lensing systems with different velocity dispersions.

within the effective radius correlate with other properties of strong lenses like their stellar density or the velocity dispersion. In particular Dutton & Treu (2014) compared the observed trends with calculated expectations based on different evolutionary scenarios for early type galaxies, such like adiabatic halo contraction, mild or no contraction or halo expansion. The trends of slope factors with the velocity dispersion found in our study (Table 1), in the case of $\alpha = \delta$ are in rough agreement with the adiabatic contraction scenario. We stress, however that the uncertainties in estimated parameters do not allow us to discriminate between

alternative behaviors. In the case of $\alpha \neq \delta$ we found no trend in central fit values – slope steepens between low-mass and intermediate-mass galaxies and then again becomes more shallow for massive galaxies. This observation should be taken with caution. First because these fits agree with each other within 1σ uncertainty. Second, because this case is hard to compare quickly against the results obtained by the others who adopted Sersic or de Vaucouleurs profiles for the light.

4 CONCLUSION

In this paper, we explored 118 strong gravitational lenses observed by SLACS, BELLS, LSD and SL2S surveys to constrain the total mass-profile and light-profile shapes of elliptical galaxies since redshift $z \sim 1$. Our method of statistical analysis is the same as in Cao et al.(2015). However, we used as a prior the best-fitted Λ CDM cosmology from Planck and assumed power-law density profiles for the total mass density, $\rho = \rho_0(r/r_0)^{-\alpha}$, and luminosity density, $\nu = \nu_0(r/r_0)^{-\delta}$. Allowing for the evolution we also investigated the total mass density profile exponent and its first derivative with respect to the redshift in the form of $\alpha = \alpha_0 + \alpha_1 z$. First, we assumed, as it was done previously by the others, that light tracers and total mass follow the same profile $\alpha = \delta = \gamma$. Then, using the full sample, we obtained $\gamma_0 = 2.132 \pm 0.055$ and a mild trend $\gamma_1 = -0.067 \pm 0.119$, suggesting that the total density profile of massive galaxies has become slightly steeper over cosmic time. Furthermore, we divided the full sample into six different sub-samples according to the lens redshifts and their velocity dispersions respectively. It turned out that there are no significant differences between lenses from different redshift bins. It is perhaps due to fact that the redshift range covered by lenses is not big enough to display any noticeable differences. However, the division according to velocity dispersion (i.e. effectively according to mass) turned out to be more discriminative. Low and intermediate mass galaxies show similar profiles ($\gamma_0 = 2.135 \pm 0.087$, $\gamma_1 = 0.012 \pm 0.204$ and $\gamma_0 = 2.115 \pm 0.072$, $\gamma_1 = -0.091 \pm 0.154$, respectively), while the best-fit values of γ_0 and γ_1 for massive galaxies ($\gamma_0 = 1.982 \pm 0.154$, $\gamma_1 = -0.047 \pm 0.350$) are significantly different from the corresponding quantities of other two sub-samples. The singular isothermal sphere model (SIS) is only consistent with results obtained in massive (high velocity dispersion) galaxies. Consequently, our results imply that the total mass density profiles of intermediate-mass and high-mass elliptical galaxies are different.

Then, we set δ as a free parameter and allow the luminosity density profile to be different from the total-mass density profile, i.e., $\alpha \neq \delta$. Performing fits on the full data and considering the redshift evolution of $\alpha = \alpha_0 + \alpha_1 z$, we obtained $\alpha_0 = 2.070 \pm 0.031$, $\alpha_1 = -0.121 \pm 0.078$, and $\delta = 2.710 \pm 0.143$. This value is also in good agreement with a recent analysis by (Schwab et al. 2010) obtained on a much smaller sample. A model in which mass traces light (i.e. $\alpha = \delta$) is rejected at $> 95\%$ confidence and our analysis robustly indicates the presence of dark matter in the form of a mass component distributed differently from the light. Fits performed on six sub-samples lead to the similar conclusion as in previous case. In particular, the substantial distinction

between α and δ admissible ranges exists in all sub-samples. It is interesting to note that only intermediate-mass elliptical galaxies are consistent with the singular isothermal sphere within 1σ , i.e. $\alpha = 2.004 \pm 0.065$. Taking the luminosity profile of elliptical galaxies into consideration, the obtained value of δ from our sub-sample with intermediate velocity dispersion is in perfect agreement with the previous results from smaller SLACS sample (Schwab et al. 2010).

As a final remark, we point out that the sample discussed in this paper is based on strong lensing systems discovered in different surveys. Our analysis potentially may suffer from systematics stemming from this inhomogeneity. If the best fitted values of α and δ power-law exponents are robustly confirmed in future larger samples, they can be used to elaborate a more accurate phenomenological model of elliptical galaxies. Such a model going beyond the SIS, would serve as a more realistic prior assumption in cosmological tests based on distance ratios.

ACKNOWLEDGMENTS

We are grateful to the referee for very constructive discussion and useful comments that allowed us to improve the paper considerably. This work was supported by the Ministry of Science and Technology National Basic Science Program (Project 973) under Grants Nos. 2012CB821804 and 2014CB845806, the Strategic Priority Research Program “The Emergence of Cosmological Structure” of the Chinese Academy of Sciences (No. XDB09000000), the National Natural Science Foundation of China under Grants Nos. 11503001, 11373014 and 11073005, the Fundamental Research Funds for the Central Universities and Scientific Research Foundation of Beijing Normal University, China Postdoctoral Science Foundation under grant No. 2015T80052, and the Opening Project of Key Laboratory of Computational Astrophysics, National Astronomical Observatories, Chinese Academy of Sciences. Part of the research was conducted within the scope of the HECOLS International Associated Laboratory, supported in part by the Polish NCN grant DEC-2013/08/M/ST9/00664 - M.B. gratefully acknowledges this support. This research was also partly supported by the Poland-China Scientific & Technological Cooperation Committee Project No. 35-4. M.B. obtained approval of foreign talent introducing project in China and gained special fund support of foreign knowledge introducing project.

REFERENCES

- Ade, P.A. R., et al. 2014, *A&A*, 571, A16
- Amanullah, R., et al. 2010, *ApJ*, 716, 712
- Auger, M. W., et al. 2009, *ApJ*, 105, 1099
- Auger, M. W., et al. 2010, *ApJ*, 724, 511
- Bartelmann, M. 1996, *A&A*, 313, 697
- Biesiada, M. 2006, *Phys. Rev. D*, 73, 023006
- Biesiada, M., Piórkowska, A., & Malec, B. 2010, *MNRAS*, 406, 1055
- Biesiada, M., Malec, B., & Piórkowska, A. 2011, *RAA*, 11, 641
- Binney, J. 1980, *MNRAS*, 190, 873

- Bolton, A. S., Rappaport, S., & Burles, S. 2006, PRD, 74, 061501
- Bolton, A. S., et al. 2008, ApJ, 682, 964
- Bolton, A. S., et al. 2012, ApJ, 757, 1
- Browne, I. W. A., et al. 2003, MNRAS, 341, 13
- Brownstein, et al. 2012, ApJ, 744, 41
- Cao, S., & Zhu, Z.-H. 2011, A&A, 538, A43
- Cao, S., Covone, G., & Zhu, Z.-H. 2012, ApJ, 755, 31
- Cao, S., Liang, N., Zhu, Z.-H. 2011, MNRAS, 416, 1099
- Cao, S., & Liang, N. 2013, IJMPD, 22, 1350082
- Cao, S., Pan, Y., Biesiada, M., Godlowski, W., & Zhu, Z.-H. 2012, JCAP, 03, 016
- Cao, S., & Zhu, Z.-H. 2012, A&A, 538, A43
- Cao, S., & Zhu, Z.-H. 2014, PRD, 90, 083006
- Cao, S., Zhu, Z.-H., & Zhao, R. 2012, PRD, 84, 023005
- Cao, S., et al., 2015, ApJ, 806, 185
- Chae, K.-H. 2003, MNRAS, 346, 746
- Chae, K.-H., & Mao, S. D. 2003, ApJ, 599, L61
- Chae, K.-H., Chen, G., Ratra, B., & Lee, D.-W. 2004, ApJ, 607, L71
- de Vaucouleurs, G. 1948, Annales d'Astrophysique, 11, 247
- Dutton, A. A., & Treu, T. 2014, MNRAS, 438, 3594
- Eisenstein, D. J., et al. 2011, AJ, 142, 72
- Fukugita, M., Futamase, T., Kasai M., & Turner, E. L. 1992, ApJ, 393, 3
- Gerhard, O., Kronawitter, A., Saglia, R. P., & Bender, R. 2001, AJ, 121, 1936
- Grillo, C., Lombardi, M., & Bertin, G. 2008, A&A, 477, 397
- Helbig, P., et al. 1999, AAS, 136, 297
- Hinshaw, G., et al. 2013, ApJS, 208, 19
- Jin, K.-J., Zhang, Y.-Z., & Zhu, Z.-H. 2000, PLA, 264,335
- Keeton, C. R. 2001, ApJ, 561, 46
- Kochanek, C. S. 1996, ApJ, 466, 638
- Kochanek, C. S., & White, M. 2001, ApJ, 559, 531
- Koopmans, L.V.E. & Treu, T. 2003, ApJ, 583, 606
- Koopmans, L.V.E., et al. 2006, ApJ, 649, 599
- Koopmans, L. V. E. 2006, in EAS Publications Series, ed. Mamon, G. A., Combes, F., Deffayet, C., & Fort, B. Vol. 20, 161
- Koopmans, L. V. E., et al. 2009, ApJ, 703, L51
- Lewis, A., & Bridle, S. 2002, PRD, 66, 103
- Lagattuta, D. J., et al. 2010, ApJ, 716, 1579
- Lauer, T. R., et al. 1995, AJ, 110, 2622
- Longair, M. S. 1998, Galaxy Formation, Springer-Verlag
- Mandelbaum, R., Seljak, U., Kauffmann, G., Hirata, C. M., & Brinkmann, J. 2006, MNRAS, 368, 715
- Mao, S. D., & Schneider, P. 1998, MNRAS, 295, 587
- Mitchell, J. L., Keeton, C. R., Frieman, J. A., & Sheth, R. K. 2005, ApJ, 622, 81
- Navarro, J. F., Frenk, C. S., & White, S. D. M. 1996, ApJ, 462, 563
- Ofek, E. O., Rix, H.-W., & Maoz, D. 2003, MNRAS, 343, 639
- Padmanabhan, N., et al. 2012, MNRAS, 427, 2132
- Ruff, A., et al. 2011, ApJ, 727, 96
- Schneider, P., Ehlers, J., & Falco, E. E. 1992, Gravitational Lenses (Springer-Verlag, New York)
- Schwab, J., Bolton, A. S., & Rappaport, S. A. 2010, ApJ, 708, 750
- Sheth, R. K., et al. 2003, ApJ, 594, 225
- Sheldon, E. S. et al. 2004, AJ, 127, 2544
- Shu, Y. P., Bolton, A. S., Brownstein, J. R., et al. 2015, ApJ, 803, 71
- Sonnenfeld, A., Gavazzi, R., Suyu, S. H., Treu, T., Marshall, P. J. 2013a, ApJ, 777, 97
- Sonnenfeld, A., Treu, T., Gavazzi, R., Suyu, S. H., Marshall, P. J., Auger, M. W., Nipoti, C., 2013b, ApJ, 777, 98
- Treu, T., & Koopmans, L.V.E. 2002, ApJ, 575, 87
- Treu, T., & Koopmans, L.V.E. 2004, ApJ, 611, 739
- Treu, T., et al. 2006a, ApJ, 640, 662
- Walsh, D., Carswell, R. F., & Weymann, R. J. 1979, Nature, 279, 381
- Zhu, Z.-H. 2000, Mod. Phys. Lett. A, 15, 1023
- Zhu, Z.-H. 2000, IJMPD, 9, 591
- Zhu, Z.-H., & Sereno, M. 2008, A&A, 487, 831
- Zhu, Z.-H., et al. 2008, A&A, 483, 15
- Zhu, Z.-H., & Wu, X.-P. 1997, A&A, 324, 483